ACS APPLIED MATERIALS & INTERFACES

Research Article

Cite This: ACS Appl. Mater. Interfaces 2018, 10, 44041−44049

www.acsami.org

Preparation of Highly Porous Polymer Membranes with Hierarchical Porous Structures via Spinodal Decomposition of Mixed Solvents with UCST Phase Behavior

Roshni L. Thankamony,[†,∥] Xiang Li,[†,∥] Xiaolin Fan,[‡] Guan Sheng,[†] Xinbo Wang,[†] Shuyu Sun,[‡] Xixiang Zhang,[§] and Zhiping Lai*[,†]

[†]Advanced Membranes and Porous Materials Centre, Chemical Engineering, Division of Physical Science and Engineering, [‡]Earth Science and Engineering, Division of Physical Science and Engineering, and [§]Material Science and Engineering, Division of Physical Science and Engineering, King Abdullah University of Science and Technology, Thuwal 23955-6900, Kingdom of Saudi Arabia

Supporting Information

ABSTRACT: The predominant method to prepare polymer membranes is based on phase inversion. However, this method always leads to a dense skin with low porosity when normal polymers are used. Using the self-assembly of certain block copolymers, it is possible to prepare uniform pores with high porosity, but the prices of these polymers are too high to be afforded in practical applications. Here, we report a novel strategy to prepare highly porous and asymmetric polymer membranes using the widely used poly(vinylidene fluoride) (PVDF) as a prototype. The method combines spinodal decomposition with phase inversion utilizing mixed solvents that have the unique upper critical solution temperature phase behavior. The spinodal decomposition generates a thin surface layer containing a high density of relatively uniform pores in the mesoporous range, and the phase inversion generates a thick bulk layer composed of macrovoids; the two types of structures are interconnected, yielding a highly permeable, selective, and mechanically strong porous membrane. The membranes show an order of magnitude higher water permeance than commercial membranes and efficient molecular sieving of macromolecules. Notably, our strategy provides a general toolbox to prepare highly porous membranes from normal polymers. By blending PVDF with cellulose acetate (CA), a highly porous PVDF/CA membrane was prepared and showed similarly high separation performance, but the higher hydrophilicity of CA improved the membrane flux in the presence of proteins.

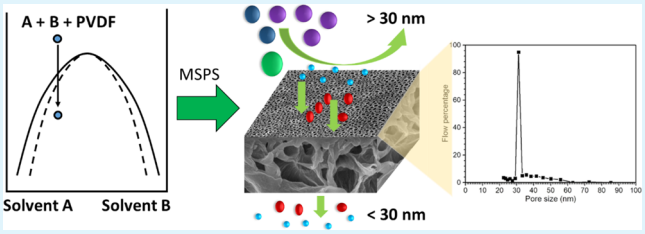

KEYWORDS: *UF membranes, spinodal decomposition, UCST, macromolecule separations, PVDF*

INTRODUCTION

Polymer membranes with hierarchical porous structures have found broad applications in filtration, adsorption, catalysis, tissue engineering, and nanotechnology.[1−3] A pore size in the range of 2−100 nm is particularly attractive because it is on the scale of many important species such as macromolecules, viruses, bacteria, colloidal particles, and nanoparticles. Membranes in such a pore size range are named as ultrafiltration (UF) membranes and have found applications in various industrial processes such as hemodialysis, food and beverage, pharmaceutical, chemical, and petrochemical, as well as in municipal water treatments.[4,5] The UF market is projected to reach USD 20 billion by 2023 with an annual growth rate of 15%.[5]

The predominant methods to prepare polymer membranes include non-solvent-induced phase separation (NIPS) and temperature-induced phase separation (TIPS).[6−13] Both methods are based on phase inversion between a solvent, in which the polymer is soluble, and a nonsolvent, usually water, in which the polymer is insoluble. The solvent and the nonsolvent are miscible with each other so that when the polymer/solvent solution is brought in contact with the nonsolvent, the nonsolvent will replace the solvent to induce phase inversion and as a consequence lead to the precipitation of the polymer to generate an asymmetric membrane structure with a dense skin layer and a macroporous bulk layer in one step. The generation of the asymmetric membrane structure is one of the most important milestones in membrane development because the membrane performance is primarily determined by the structure of the skin layer, while the thick bulk layer provides enough mechanical strength.[14] However, to the best of our knowledge, which is also supported by other reports,[6,15] all of the reported polymer membranes prepared out of normal polymers have either high porosity but large pore size (>250 nm) or low porosity (<2%) in the UF pore size range. The low porosity has greatly limited the water permeance of UF membranes, which is typically less than 100 LMH/bar. The only reported efficient way to prepare highly

Received: September 16, 2018
Accepted: November 20, 2018
Published: November 20, 2018

DOI: 10.1021/acsami.8b16120
ACS Appl. Mater. Interfaces 2018, 10, 44041−44049

porous UF membranes is to use the self-assembly of block copolymers (SABCP) that contain blocks with different properties.[16−26] The SABCP method can generate an almost ideal membrane structure, i.e., high porosity, uniform pore size, and thin skin. It can also combine with the phase inversion process to prepare UF membranes in large scale. However, block copolymers are expensive, and their stability is poor. Furthermore, the porous structure of block copolymer membranes is strongly dependent on many factors such as the type of polymer blocks, the total molecular weight, the ratio of the blocks, and polydispersity.[19−23] All of these requirements pose significant challenges in polymer design and synthesis.

On the other hand, the widely used polymers in practical applications are normal polymers such as poly(vinylidene fluoride) (PVDF), cellulose acetate (CA), polysulfone, and poly(ethersulfone).[5] These polymers have good chemical and mechanical stabilities and are cheap. However, as mentioned above, the UF membranes prepared out of these polymers always have a dense skin with very low porosity. Hence, it is highly desirable to develop a new method to prepare UF membranes out of these normal polymers with the surface porous structure similar to that of the SABCP method. Here, we propose a novel strategy to reach close to this goal by combining the spinodal decomposition with phase inversion. Our key idea is to use a mixed solvent system that has an upper critical solution temperature (UCST). The polymer should be soluble only in one solvent but not the other. The UCST behavior allows the mixed solvent system and the polymer to form a homogeneous solution at high temperatures; however, when the temperature switches below the critical point, the mixed solvent phase separates via spinodal decomposition to generate regular nanodomains. During this process, the polymer migrates to the soluble solvent domains and becomes concentrated. The membrane is then immersed in a nonsolvent bath (e.g., water), which precipitates the polymer and removes the solvents. Finally, a porous membrane with a high density of surface pores is obtained. We name this process "mixed solvent phase separation" (MSPS).

We found a common solvent used for the preparation of polymer membranes, *N*,*N*-dimethylformamide (DMF), which can form UCST systems with alkanes.[27] Luckily, most of the normal polymers are not soluble in alkanes. Hence, in this study, we used DMF and octane as the prototype mixed solvent system. We demonstrated our concept by using PVDF as our prototype polymer. However, PVDF is hydrophobic and known to be prone to fouling.[28] Hence, we also tried to blend PVDF with cellulose acetate (CA) to use the hydrophilicity of CA to improve the antifouling performance and demonstrate the adaptive capability of the method.

EXPERIMENTAL SECTION

Materials. Poly(vinylidene fluoride) was purchased from 3M (Dyneon PVDF 6133). Cellulose acetate was purchased from Eastman (CA-398-30). *N*,*N*-Dimethylformamide (DMF, >99.8), octane (>99%), nonane (>99%), and isopropyl alcohol (IPA, >99%) were purchased from Fisher Scientific. Bovine serum albumin (BSA), γ-globulin (IgG), and phosphate-buffered saline (PBS) were acquired from Sigma-Aldrich. Poly(ethylene oxide) (PEO) with different molecular weights (10k, 35k, 60k, 100k, 180k, 230k, and 380k) was purchased from Polymer Source, Inc. All reagents and chemicals are of analytical grade and used as received. Deionized (DI) water is purified by a Milli-Q system (Millipore, Inc.).

Phase Diagram Determination. The phase equilibrium was determined visually by observing the cloud points through a simple titration method. For the DMF/octane system, a known amount of DMF in a flask was placed in an isothermal bath with a temperature accuracy of 0.1 °C and then titrated with octane. The amount of octane required to bring the onset of the next turbidity point was measured with a precision of 0.01 g. The molar fraction and the temperature at each turbidity point represented a phase equilibrium point. The molar fractions of the equilibrium points at different temperatures of the DMF/octane system are listed in Table S1 (Supporting Information).

Preparation of MSPS Membranes. The MSPS PVDF membrane was prepared by mixing 15 wt % PVDF in 55 wt % DMF and 30 wt % octane at 85 °C to form a homogeneous casting solution. A thin film was cast on a glass plate by a doctor blade with 200 μm air gap inside a hot chamber at 85 °C. The film was covered by a glass container and left at room temperature. The surface temperature was monitored by an IR thermometer. After 1 min waiting, the membrane was immersed in a room-temperature DI water coagulation bath until it was detached. The membrane was then taken out and kept in another fresh DI water for 24 h to remove any trace of solvent. The wet membranes were used directly for the filtration tests and pore size measurements. For other characterizations, the membranes were washed with IPA several times and then dried at ambient conditions. The dry membrane showed white color and was opaque. The average membrane thickness was measured at 10 different points by a micrometer. MSPS PVDF/CA membranes were prepared in a similar way, except that the casting solution contained 7.41 wt % PVDF, 7.41 wt % CA, 59.26 wt % DMF, and 25.93 wt % octane, and the casting temperature was 90 °C. For comparison, PVDF and PVDF/CA membranes were also prepared by the NIPS process in which DMF was used as a single solvent. In the standard NIPS process, membrane casting was conducted at room temperature. However, for better comparison, we have also followed the same temperature process as the MSPS process to prepare the membranes. It was found that the membranes prepared by these two NIPS processes had almost identical membrane structures. The reason is probably because the temperature used in the MSPS process is quite low compared to that in the normal TIPS processes (∼200 °C).[10,13]

Membrane Characterization. Scanning electron microscopy (SEM) images were obtained from a Nova Nano FESEM at an accelerating voltage of 3 kV. The samples were sputter-coated with iridium before observation. The water contact angle was measured by a contact angle goniometer (FM40, KRÜSS GmbH, Germany) equipped with a video recorder. For static and dynamic contact angle measurements, 2 μL of DI water was dropped onto the membrane surface and the sessile drop method was used to obtain the contact angle values. Images of the water droplets were captured using a video camera (Stingray model, Allied Vision Technology). To minimize the experimental error, the contact angle was measured at least at four random locations of the membrane, and the average values were reported.

Fourier transform infrared (FTIR) spectroscopy was conducted by a Nicolet iS10 smart FTIR spectrometer (Thermo Scientific) equipped with a smart OMNI transmission ranging from 400 to 4000 cm^{-1}. The XRD patterns were measured on a Bruker AXS D8 focus advanced X-ray diffractometer operated at 40 kV and 40 mA using Cu Kα radiation of wavelength λ = 1.5406 Å. Before measurement, the equipment was calibrated by a standard silicon sample (Rigaku, Japan, Tokyo).

The thermal behavior of the membrane samples was characterized by a differential scanning calorimetry (DSC) device (Q-2000, TA Instruments) from −25 to 250 °C at 10 °C/min heating rate. From the DSC results, the degree of crystallinity of the PVDF membranes was calculated by the following equation

$$\%\ \text{crystallinity} = \frac{\Delta H_m}{\Delta H_m^\circ} \times 100\% \quad (1)$$

DOI: 10.1021/acsami.8b16120
ACS Appl. Mater. Interfaces 2018, 10, 44041−44049

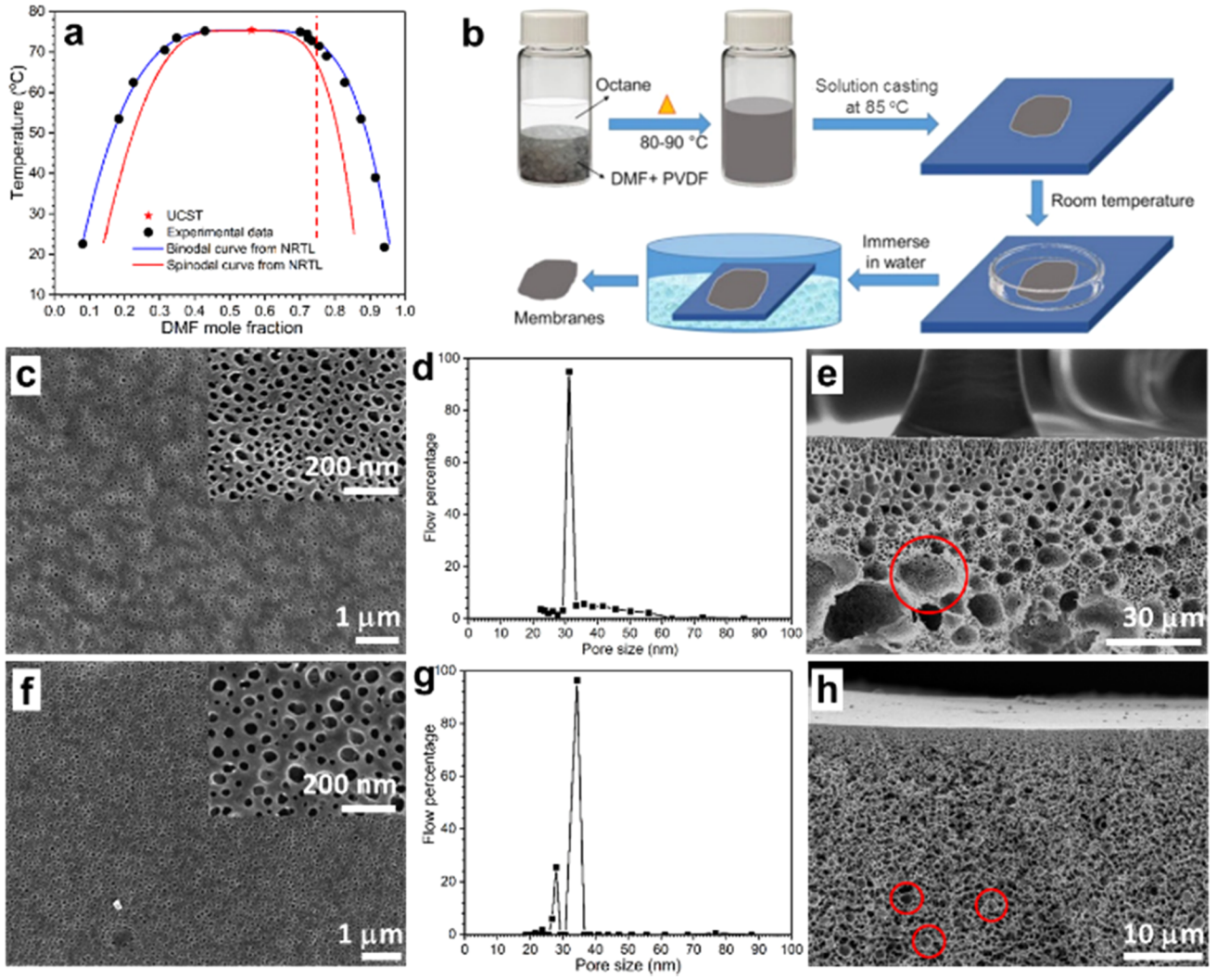

Figure 1. (a) DMF and octane phase diagram. The red vertical dashed line indicates the mole fraction of DMF in the casting solution and phase evolution during the membrane casting procedure. (b) Schematic of the MSPS membrane fabrication process. (c) Top view of the MSPS PVDF membrane. The inset shows a magnified image. (d) Pore size distribution of the MSPS PVDF membrane. (e) Cross section of the MSPS PVDF membrane. (f) Top view of the MSPS PVDF/CA membrane. The inset shows a magnified image. (g) Pore size distribution of the MSPS PVDF/CA membrane. (h) Cross section of the MSPS PVDF/CA membrane.

where ΔH_m is the heat associated with melting (fusion) of the sample and obtained from the DSC thermogram and ΔH_m° is the heat of melting if the polymer is 100% crystalline, which is 104.7 J/g for the PVDF polymer.

The mechanical properties of the membranes were tested according to International Organization for Standardization (ISO) 527-2, using a tensile testing machine, Instron 5882. The membrane samples were cut into the standard dog-bone shape using a super dumbbell cutter. The sample thickness was measured by a micrometer. The sample was fixed at a gauge length of 30 mm and then stretched at a constant rate of 10 mm/min. The corresponding tensile force and elongation were recorded until breaking. At least five samples were tested for each type of membranes.

The membrane pore size distribution was measured by gas−liquid displacement porosimetry using a POROLUX 1000 device (POROMETER, Belgium). The membranes were cut into certain size and wetted with a special wetting liquid, POREFIL, which is provided by the supplier and has a surface tension of 16 mN/m. After loading the sample into the porometer, N_2 gas was applied from one side of the membrane sample and the pressure was increased from 0 to 34.5 bar step by step to replace the wetting liquid inside the membrane pores. The data were recorded when both the pressure and the flow rate were stabilized within ±1% accuracy for 2 s at each step. The Young−Laplace equation was employed to calculate the pore size corresponding to each operation pressure as follows

$$d = \frac{4\gamma \cos\theta}{\Delta P} \tag{2}$$

where d is the diameter of the pores that contribute to the gas flow at each operation pressure; γ is the surface tension of the wetting liquid, which is 16 mN/m; θ is the contact angle of the wetting liquid on the membrane surface, which is 0°; and ΔP is the specific operation pressure. The mean flow pore diameter and pore size flow distribution were obtained.

Flux and Retention Measurement. The pure water flux was tested by a homemade ultrafiltration permeation cell operated in the dead-end mode. A membrane with an effective surface area of 2.3 cm^2 was placed first over a nonwoven fabric support and then over a porous stainless steel support and sealed by O-ring. The feed side of the cell was pressurized by N_2 gas from a cylinder. The permeate water was collected and measured by a digital balance. The water permeance was calculated as follows

$$P = \frac{V}{A \times t \times \Delta p} \tag{3}$$

DOI: 10.1021/acsami.8b16120
ACS Appl. Mater. Interfaces 2018, 10, 44041−44049

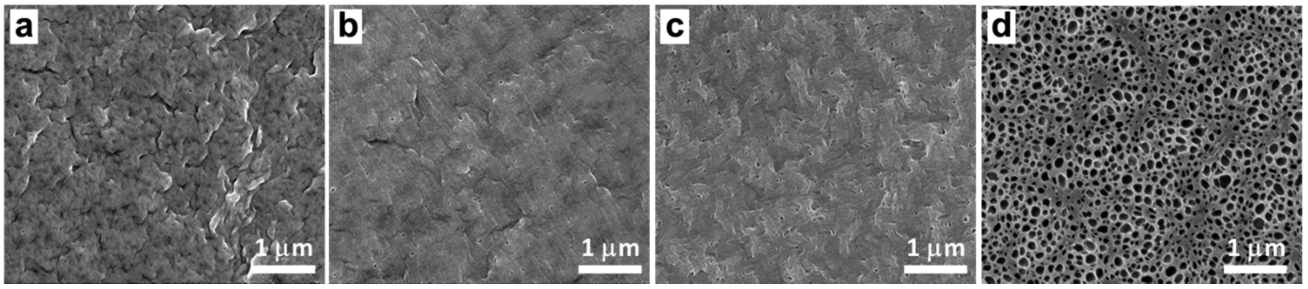

Figure 2. Comparison of membranes formed in different solvent systems: (a) DMF alone, (b) DMF/pyridine, (c) DMF/toluene, and (d) DMF/nonane.

where V is the volume of the collected DI water (L) during the permeation time t (h); A is the effective membrane area (m^2); and Δp is the transmembrane pressure drop (bar).

The molecular weight cutoff was measured using poly(ethylene oxide) (PEO) with different molecular weights as probe molecules. The molecular size of PEO was estimated by the following Stokes–Einstein relationship[29]

$$d_H = \frac{K_B T}{3\pi\mu D_0} \quad (4)$$

$$D_0 = 1.79 \times 10^{-4} \times M_w^{-0.587} \quad (5)$$

where d_H is the hydrodynamic diameter of the molecule (nm); K_B is the Boltzmann constant; T is the temperature (K); μ is pure solvent viscosity (Pa s); D_0 is the diffusion constant (cm^2/s); and M_w is the molecular weight (g/mol). PEO was dissolved in DI water at a concentration of 100 ppm and then filtered through the membranes at 0.5 bar using the same ultrafiltration cell in the flux measurements in the dead-end mode. The feed and the permeate concentrations were measured by gel permeation chromatography (Agilent 1200 series system) using DI water as an eluent. The rejection rate (R, %) of the membrane for each PEO is calculated by the following equation

$$R(\%) = \left(1 - \frac{C_p}{C_f}\right) \times 100 \quad (6)$$

where C_p and C_f are the concentrations at the permeate and feed solutions, respectively.

The membrane capability to separate different proteins was demonstrated using two common proteins, bovine albumin (BSA) and γ-globulin (IgG). BSA and IgG solutions (100 ppm) stabilized in a commercial PBS buffer solution at a physiological pH of 7.4 were used as feed solutions and filtered through the membranes at 0.5 bar in the same way as the PEO rejection measurements. The protein concentrations in the feed and permeate streams were measured by a UV–visible spectrophotometer (Varian Cary 5000) at λ_{max} = 280 nm. The rejection rate of proteins was calculated by eq 6. For the membrane stability testing, Amicon 8010 cell with a reservoir of 10 L DI water was used. A membrane with effective surface area of 4.1 cm^2 was adopted, and the feed side of the cell was pressurized at 1.0 bar. The flux was recorded after 5 min of pressurization.

RESULTS AND DISCUSSION

The DMF/octane phase diagram is shown in Figure 1a. The diagram is similar to that reported in the literature.[27] The phase diagram has a UCST point around 75 °C. Fitting the equilibrium data points by a nonrandom two-liquid (NRTL) model (Section 1, Supporting Information) gives the binodal curve (blue line) and the spinodal curve (red line). On the basis of this phase diagram, we developed the membrane preparation procedure illustrated in Figure 1b. First, a homogeneous solution of DMF, octane, and PVDF was formed above 85 °C. The red dashed line indicates the composition of the mixed solvent in the phase diagram, where the mole fraction of DMF is 74%. The membrane was cast at 85 °C through the standard solution casting procedure. The membrane was then covered by a glass container to avoid overevaporation in the surface and then left at room temperature and waited for a certain period of time to allow the temperature to drop below the critical point to initiate phase separation. In a typical process, the surface temperature dropped to 60 °C after waiting for 1 min. Afterward, the membrane was immersed in a room-temperature water bath to form a solidified membrane.

Figure 1c shows the top-view SEM image of the PVDF membrane prepared by MSPS. The PVDF membrane contained a high density (estimated to be 2.1 × 10^{14} m^{-2}) of surface pores. The surface porosity was around 21%. The pore size appears less uniform than the SABCP membranes in the SEM images. However, the size distribution determined by gas–liquid displacement porosimetry in Figure 1d showed a sharp distribution with an average pore size around 31 ± 2 nm. Both the surface porosity and size uniformity are much better than the membranes prepared by the normal phase inversion methods.[6] A cross-sectional SEM image of the membrane is shown in Figure 1e. The total membrane thickness was around 65 ± 8 μm. The bulk phase had a very hierarchical porous structure, and the surface layer was very thin. A close look into the surface layer (Figure S4, Supporting Information) indicates that it opened up immediately to the bulk layer. Below the surface layer, there were two types of nanostructures: coarse spherical pores and fine, spongelike structures. The size of the spherical pores increased gradually from top to bottom, whereas the size of the spongelike structure was uniform. The area highlighted by the red circle in Figure 1e shows that the two types of structures were interconnected. The membrane made of PVDF blended with CA (denoted PVDF/CA) had a similar high density of surface pores (estimated to be 7.5 × 10^{13} m^{-2}, Figure 1f). The pore size distribution, like that of PVDF, was narrow, although less uniform (Figure 1g). In addition to the main peak centered at 34 ± 3 nm, a minor peak appeared at 28 ± 2 nm. However, the bulk structure of the PVDF/CA membrane was much more uniform. The bulk structure contained the spherical pores again, as highlighted by the circles in Figure 1h, and the spongelike structures, but the sizes of these two nanostructures are much close to each other.

We hypothesize that the surface pores were generated by spinodal decomposition of the mixed solvents because the surface temperature dropped quickly below the spinodal curve during the membrane fabrication process. Because spinodal decomposition is far from thermodynamic equilibrium and has no thermal energy barrier, it is expected to occur quickly and uniformly. Hence, when octane separates from DMF, it forms

DOI: 10.1021/acsami.8b16120
ACS Appl. Mater. Interfaces 2018, 10, 44041–44049

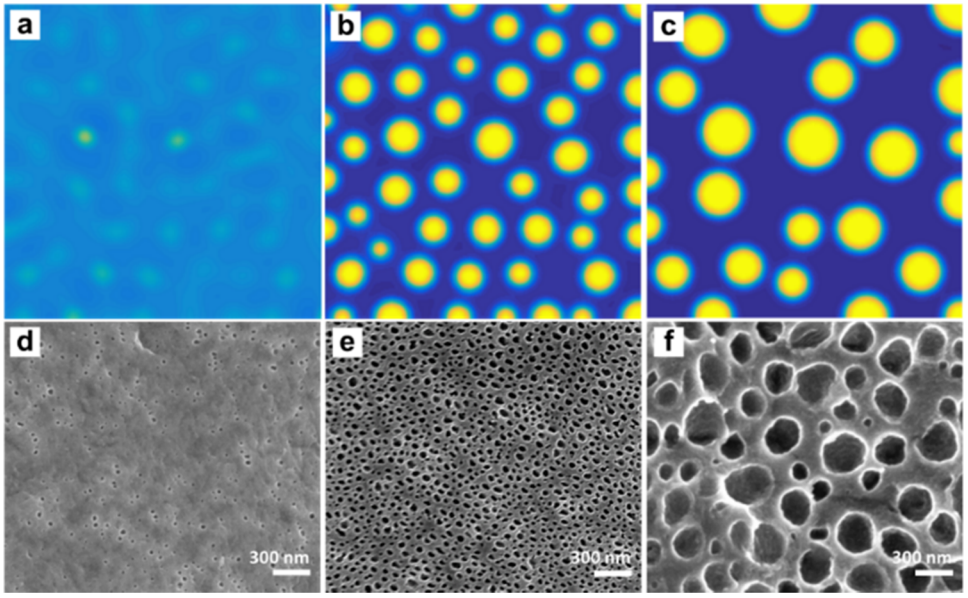

Figure 3. Top three images are simulated patterns at different evolution steps: (a) 10 000, (b) 20 000, and (c) 60 000 times, based on the CH equation. The equivalent time interval was 3×10^{-3} s. The temperature was set to 60 °C. A homogeneous Neumann boundary condition and a random initial condition $\phi_0 + r(200, 200)$ were applied, where $\phi_0 = 0.57$, representing the volume fraction of DMF, and $r(200, 200)$ was a random matrix with each entry generated from the normal distribution $N(0, 10^{-8})$, representing thermal fluctuations. The bottom three images are the MSPS PVDF membranes prepared at different waiting times of (d) 0.5, (e) 1, and (f) 3 min.

local spherical domains, whereas DMF (as the major component) forms the continuous phase. PVDF migrates to the DMF phase because it is soluble in DMF only. When the membrane comes into contact with water, PVDF condenses and forms a dense skin in the DMF region. The bulk phase of the membrane is formed by two processes: phase separation between octane and DMF and phase inversion between DMF and water. First, octane separates from DMF and forms discrete spherical pores, and DMF and PVDF form the continuous phase. Then, as water diffuses into the bulk phase, it replaces DMF and precipitates PVDF, forming the spongelike structure. The size of the spherical pores increases gradually from top to bottom. This is because PVDF is hydrophobic, so the diffusion of water is slow, which allows octane at the bottom to form larger domains. In contrast, PVDF/CA is more hydrophilic (confirmed by the contact angle measurements in Figure S5 and dynamic contact angle measurements in Figure S6, Supporting Information); thus, water enters very quickly, which leads to a much more uniform structure.

To verify our hypothesis, PVDF membranes were prepared in four different types of solvent systems following the same MSPS procedure. The first case is DMF alone (Figure 2a), which is essentially the standard NIPS process. The second case is DMF/pyridine (Figure 2b), where pyridine is completely miscible with both DMF and water. The third case is DMF/toluene (Figure 2c), where toluene is completely miscible with DMF but immiscible with water. The fourth case is DMF/nonane (Figure 2d), which is another UCST mixed solvent system with a critical temperature of around 80 °C. As shown in Figure 2, the membranes made in the first three solvent systems were dense with very low pore densities, which were consistent with the reported PVDF membranes prepared by the standard NIPS and TIPS methods. However, the membrane made in DMF/nonane showed again a highly porous structure on the surface, similar to the DMF/octane system. Thus, we confirmed that only a mixed solvent with the UCST phase behavior could form high density of uniform pores on the membrane surface.

To further confirm the mechanism, we simulated the spinodal decomposition process using the Cahn–Hilliard (CH) model coupled with the Flory–Huggins free energy density (Section 3, Supporting Information).[30] A noise term was added to the CH model to mimic disturbances due to thermal fluctuations. The simulation adopted a time step size of 3×10^{-3} s. The process is kinetically controlled, hence the pattern changes with time. Figure 3a–c shows the simulated patterns at different evolution steps, 10 000, 20 000, and 60 000, which correspond to time periods 0.5, 1, and 3 min. Figure 3d–f shows the MSPS PVDF membranes prepared at the same time periods.

In the simulation, the phase diagram information was retrieved from Figure 1a. However, adding polymer may affect the phase diagram, so a strict simulation will be needed to consider the system as three components. Also, due to the lack of thermodynamic data for the DMF/octane system, empirical values were used for the parameters used in the NRTL model and the Flory–Huggins equation. Hence, it is expected that the simulated pattern size will be different from the experimental ones, but the structure of the pattern and the trend of its evolution with time should be similar if the pattern is formed due to spinodal decomposition of DMF and octane, which is indeed the situation by comparison between the two types of patterns. In both cases, the pores are small, and the density is low at short time period. The simulated pattern clearly indicates that the reason is because at this stage, the two solvents have not separated completely; only the centers of a few spots have sufficient intensity to generate pores. With increase in time (reaching the middle stage), the intensity of the pattern becomes stronger and the density increases. With further increase in time, the pattern size increases, but the density decreases. This is because the neighboring pattern

DOI: 10.1021/acsami.8b16120
ACS Appl. Mater. Interfaces 2018, 10, 44041–44049

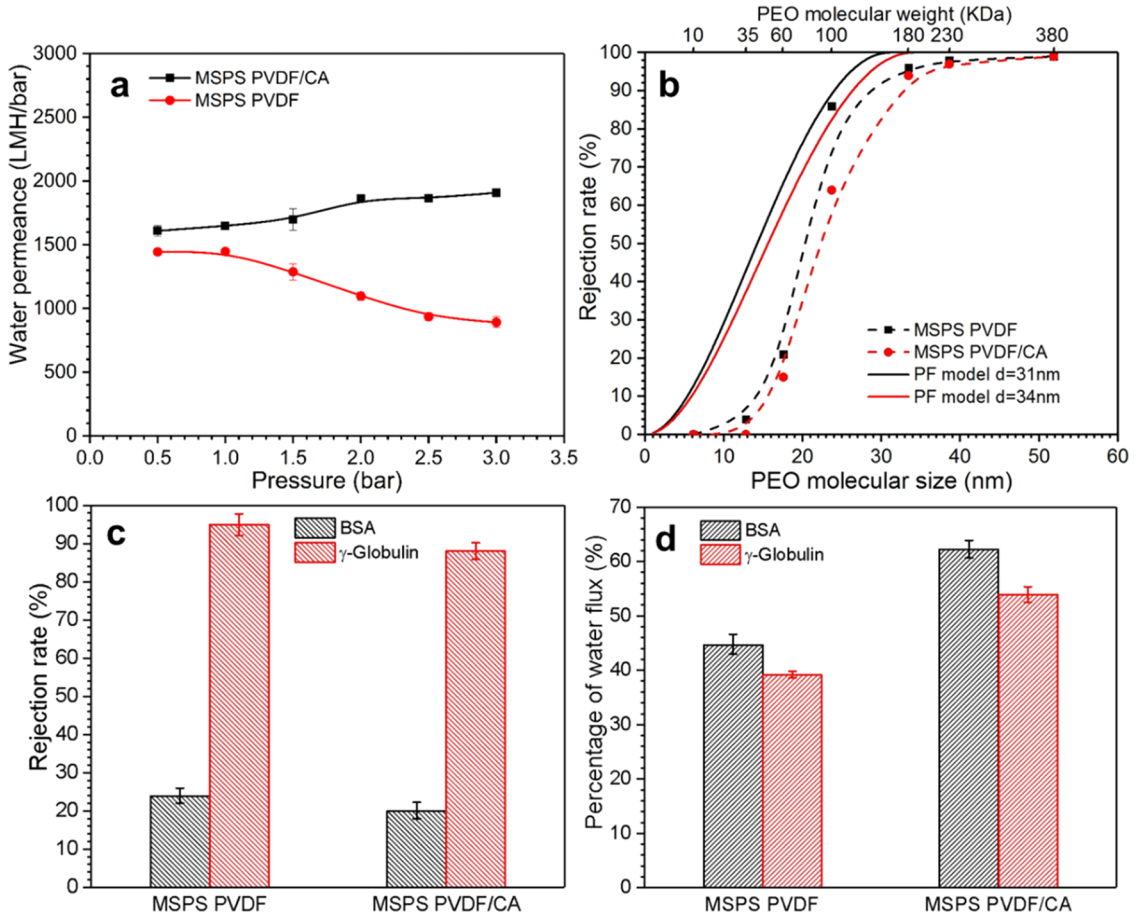

Figure 4. (a) Pure water permeance of the MSPS PVDF and MSPS PVDF/CA membranes at different applied pressures. (b) Rejection rate of PEO molecules at different molecular weights (top axis) and molecular sizes (bottom axis) of the MSPS PVDF and MSPS PVDF/CA membranes. (c) Rejection rate of BSA and γ-globulin on the MSPS PVDF and MSPS PVDF/CA membranes. (d) Water flux in the presence of proteins BSA and γ-globulin compared to the pure water flux. The test conditions are BSA and γ-globulin concentrations of 100 ppm and an applied pressure of 0.5 bar.

domains coarsened each other, forming larger, but fewer, pores. Therefore, the simulation results confirmed that the spinodal decomposition between DMF and octane is the main mechanism for the pattern formation. The simulation results also indicated that the random noise was the source of the nonuniformity that was observed in both simulated patterns and real porous structures. When a periodic initial setting and a tiny disturbance were applied to the CH model, as shown in Figure S3, the simulated pattern was very uniform, implying that a uniform porous structure could be obtained if all of the experimental conditions are well controlled.

The membrane chemical structure, crystallinity, and thermal properties are characterized by Fourier transform infrared (FTIR, Figure S7) spectroscopy, X-ray diffraction (XRD, Figure S8), and differential scanning calorimetry (DSC, Figure S9). These results show that the membrane properties prepared by MSPS are close to those prepared by the normal NIPS process, either prepared in this study or reported in the literature.[15,31,32] The mechanical properties of the MSPS PVDF membrane were measured by tensile tests following the standard ISO 527-2 method (Figure S10). A tensile strength of 6.8 MPa with a ductility of around 50% was obtained. Again, these mechanical properties are among the range of the reported PVDF membranes prepared by the NIPS method.[15,32,33] The reason why the properties of the MSPS membranes are close to those of the NIPS membranes is probably because the temperature used in the MSPS process is low compared to the temperature used in the TIPS processes (~200 °C).[10,13]

The permeation properties of the MSPS PVDF and MSPS PVDF/CA membranes are shown in Figure 4. The water permeances at low pressure were about 1400 ± 45 LMH/bar for MSPS PVDF and around 1600 ± 64 LMH/bar for MSPS PVDF/CA. The water permeance of the MSPS PVDF membrane decreased gradually to about 900 LMH/bar when the pressure increased from 1 to 3 bar due to structure compression.[12,13,34] The water permeance of MSPS PVDF/CA was much more stable. It even slightly increased with increase in pressure. This is most likely due to the much more uniform bulk structure.[4] Many UF membranes suffered from a serious flux reduction in the initial stage of running, particularly in the first 2 h.[15,22,35−43] Hence, Figure S12 shows long-term tests over 5 h on both MSPS PVDF and MSPS PVDF/CA membranes, and the results showed that the water permeances of both membranes were stable during the studied periods. The effective membrane thickness was calculated using the Hagen−Poiseuille equation, which yielded 1.4 μm for the MSPS PVDF membrane and 0.73 μm for the MSPS PVDF/CA membrane. The effective membrane thickness was less

DOI: 10.1021/acsami.8b16120
ACS Appl. Mater. Interfaces 2018, 10, 44041−44049

Table 1. Performance Comparison with Membranes Made of Block Copolymers and with Commercial Membranes with Similar Pore Sizes

entry	membranes	method or manufacturer	average pore size (nm)	pore density or porosity	pure water permeance (LMH/bar)	ref
1	PS_{138}-*b*-P_4VP_{41}	SABCP	30	2.3×10^{14}	890	24
2	PS_{175}-*b*-P_4VP_{65}	SABCP	34	2.2×10^{14}	3200	25
3	PS_{138}-*b*-PEO_{18}	SABCP	40	3.2×10^{14}	800	19
4	PS_{81}-*b*-P_4VP_{19}	SABCP	34 ± 4	25.8%	400	26
5	PS_{74}-*b*-P_4VP_{26}	SABCP	38	2.47×10^{14}	625	23
6	PVDF−PEG	CCD	38 ± 2		1384	15
7	PCN3CP04700	Track-etching	30	0.4%	211	44
8	IntegraFlux	Dow Corp.	30		40−120	15
9	EnviQ	QUA Corp.	40		20	15
10	PURON	Koch Corp.	30		100	15
11	PV200	Nanostone Corp.	45		153	45
12	PVDF	NIPS	30		<10	this work
13	PVDF	MSPS	31 ± 2	2.1×10^{14}, 21%	1400	this work
14	PVDF−CA	MSPS	34 ± 3	7.5×10^{13}	1600	this work

than 2% of the real membrane thickness, clearly indicating the advantage of the asymmetric membrane structure.

Figure 4b shows the size exclusion of the MSPS membranes using different molecular weights of poly(ethylene oxide) (PEO) as the probe molecules. Both MSPS PVDF and MSPS PVDF/CA membranes allowed almost all PEO molecules with size less than 14 nm to pass through. The molecular size cutoff of the membranes is defined as a rejection rate of 90%, which, determined from Figure 4b, is about 29 nm for MSPS PVDF and 33 nm for MSPS PVDF/CA. The molecular size cutoff of both membranes is consistent with the average pore size measured by the gas−liquid displacement porosimetry. In Figure 4b, the rejection rates predicted by the pore flow model (Section 2, Supporting Information) assuming a uniform pore size equal to the average pore size of the membranes are shown as solid lines. The predicted transition ranges in both cases moved to a lower size range compared to the real situations, which is probably because the model is based on rigid membrane structures and rigid particles, whereas in real situations, both the membrane and PEO molecules are flexible. However, the shape and width of the transition ranges of the MSPS membranes are similar to the model predictions, which indicate a sharp size exclusion effect.

An important application of ultrafiltration is protein separation. This is shown in Figure 4c. The MSPS PVDF and MSPS PVDF/CA membranes rejected about 90% of the large γ-globulin protein but only 20% of the smaller bovine serum albumin (BSA) protein. One disadvantage of the PVDF membrane in protein separation is that it is prone to fouling because of its high hydrophobicity.[28] As shown in Figure 4d, in the presence of BSA and γ-globulin, the water flux dropped to about 40% of the pure water flux. An effective approach to mitigate fouling is to increase the hydrophilicity.[28] Because blending CA with PVDF increases the hydrophilicity of the membrane, under the same conditions, the water flux of the MSPS PVDF/CA membrane was improved to about 60% of the pure water flux. The cyclability of the membrane is briefly demonstrated in Figure S13. The MSPS PVDF membrane was cleaned by sonication after BSA filtration. The water flux was repetitively recovered from 40 to 60% in three consecutive cycles.

To compare the membrane performance, the best reference is SABCP membranes because they represent the state-of-the-art performance. The first five entries of Table 1 list the reported block copolymer membranes with pore sizes similar to those of the MSPS membranes. The MSPS PVDF and MSPS PVDF/CA membranes have similar pore densities or porosities and water permeances as these block copolymer membranes. Table 1 also lists a recently reported high-flux membrane made by a novel crystallization and diffusion (CCD) procedure (entry 6). Again, the permeance is equivalent to the permeances of MSPS membranes. The rest of the membranes listed in Table 1 are commercial UF membranes with similar pore sizes, which are prepared by either the standard NIPS or TIPS methods, and the PVDF and PVDF/CA membranes prepared by the NIPS and MSPS processes in this study. All of the commercial membranes and the NIPS PVDF membrane have permeances at least 1 order of magnitude lower than the MSPS membranes, which clearly demonstrated the advantage of the MSPS method.

CONCLUSIONS

An MSPS process was successfully developed, which utilized the unique UCST mixed solvent behavior to combine spinodal decomposition with phase inversion to prepare asymmetric polymer membranes with an ultrathin surface layer containing a high density of narrowly distributed pores and a thick bulk layer composed of macrovoids in one step. The MSPS PVDF membranes had a pore size around 31 nm, a pore density of 2.1×10^{14}, a surface porosity of 21%, and a water permeance of 1400 LMH/bar, and the MSPS PVDF/CA membranes had a pore size around 34 nm, a pore density of 7.5×10^{13}, and a water permeance of 1600 LMH/bar. Although the pore size is less uniform than the SABCP method, both membranes showed good size exclusion for separation of macromolecules and proteins, indicating that the pore size uniformity is satisfactory for practical applications. The MSPS PVDF/CA membrane showed higher water flux in the presence of proteins, implying the potential for better antifouling performance because of its higher hydrophilicity, compared to the PVDF membranes. The pore size, surface porosity, and the permeation performance of the MSPS membranes are all equivalent to those of SABCP membranes, but an order of magnitude higher than conventional membranes. Compared to the SABCP method, the MSPS method shifts the self-assembly from the polymer to the solvent; hence, any conventional polymer could be used in principle. The MSPS procedure is

DOI: 10.1021/acsami.8b16120
ACS Appl. Mater. Interfaces 2018, 10, 44041−44049

similar to the widely used temperature-induced phase separation (TIPS) technique and, thus, can be scaled up easily.

■ ASSOCIATED CONTENT

Supporting Information

The Supporting Information is available free of charge on the ACS Publications website at DOI: 10.1021/acsami.8b16120.

NRTL model, the pore flow model, simulation of the spinodal decomposition process, and the results of phase diagram, SEM image, contact angle measurement, FTIR, XRD, DSC, mechanical properties, and stability tests (PDF)

■ AUTHOR INFORMATION

Corresponding Author

*E-mail: Zhiping.lai@kaust.edu.sa.

ORCID

Xiang Li: 0000-0002-5656-1363
Xixiang Zhang: 0000-0002-3478-6414
Zhiping Lai: 0000-0001-9555-6009

Author Contributions

The manuscript was written through contributions of all authors. All authors have given approval to the final version of the manuscript.

Author Contributions

‖R.L.T. and X.L. contributed equally to this work.

Funding

This work was supported by KAUST baseline fund BAS/1/1375.

Notes

The authors declare no competing financial interest.

■ ACKNOWLEDGMENTS

The authors thank Dr M. Karunakaran for the help in protein tests, Prof. I. Pinnau for useful discussions on the mechanism of spinodal decomposition, Prof. S.P. Nunes for the pore size distribution measurements, and Prof. G. Lubineau for the tensile test.

■ ABBREVIATIONS

UF, ultrafiltration
SEM, scanning electron microscopy
UCST, upper critical solution temperature
MSPS, mixed solvent phase separation
SABCP, self-assembly of block copolymers
NIPS, non-solvent-induced phase separation
TIPS, temperature-induced phase separation
PVDF, poly(vinylidene fluoride)
CA, cellulose acetate
DMF, *N*,*N*-dimethylformamide
PEO, poly(ethylene oxide)
BSA, bovine serum albumin
CCD, crystallization and diffusion

■ REFERENCES

(1) Yoo, S.; Kim, J. H.; Shin, M.; Par, H.; Kim, J. H.; Lee, S. Y.; Park, S. Hierarchical Multiscale Hyperporous Block Copolymer Membranes Via Tunable Dual-Phase Separation. *Sci. Adv.* **2015**, *1*, No. e1500101.

(2) Sai, H.; Tan, K. W.; Hur, K.; Asenath-Smith, E.; Hovden, R.; Jiang, Y.; Riccio, M.; Muller, D. A.; Elser, V.; Estroff, L. A.; Gruner, S. M.; Wiesner, U. Hierarchical Porous Polymer Scaffolds from Block Copolymers. *Science* **2013**, *341*, 530−534.

(3) Tsurusawa, H.; Russo, J.; Leocmach, M.; Tanaka, H. Formation of Porous Crystals Via Viscoelastic Phase Separation. *Nat. Mater.* **2017**, *16*, 1022−1029.

(4) Baker, R. W. *Membrane Technology and Applications*, 3rd ed.; John Wiley & Sons, Inc.: Hoboken, NJ, 2012.

(5) MarketsandMarkets.com Ultrafiltration Market - Global Forecast to 2023. http://www.marketsandmarkets.com (accessed September 10, 2018).

(6) Lalia, B. S.; Kochkodan, V.; Hashaikeh, R.; Hilal, N. A Review on Membrane Fabrication: Structure, Properties and Performance Relationship. *Desalination* **2013**, *326*, 77−95.

(7) Wienk, I. M.; Boom, R. M.; Beerlage, M. A. M.; Bulte, A. M. W.; Smolders, C. A.; Strathmann, H. Recent Advances in the Formation of Phase Inversion Membranes Made from Amorphous or Semi-Crystalline Polymers. *J. Membr. Sci.* **1996**, *113*, 361−371.

(8) Guillen, G. R.; Pan, Y.; Li, M.; Hoek, E. M. V. Preparation and Characterization of Membranes Formed by Nonsolvent Induced Phase Separation: A Review. *Ind. Eng. Chem. Res.* **2011**, *50*, 3798−3817.

(9) Zhang, P. Y.; Yang, H.; Xu, Z. L. Preparation of Polyvinylidene Fluoride (PVDF) Membranes Via Nonsolvent Induced Phase Separation Process Using a Tween 80 and H_2O Mixture as an Additive. *Ind. Eng. Chem. Res.* **2012**, *51*, 4388−4396.

(10) Cui, Z.; Hassankiadeh, N. T.; Lee, S. Y.; Lee, J. M.; Woo, K. T.; Sanguineti, A.; Arcella, V.; Lee, Y. M.; Drioli, E. Poly(Vinylidene Fluoride) Membrane Preparation with an Environmental Diluent via Thermally Induced Phase Separation. *J. Membr. Sci.* **2013**, *444*, 223−236.

(11) Wang, D.-M.; Lai, J. Y. Recent Advances in Preparation and Morphology Control of Polymeric Membranes Formed by Non-solvent Induced Phase Separation. *Curr. Opin. Chem. Eng.* **2013**, *2*, 229−237.

(12) Jung, J. T.; Kim, J. F.; Wang, H. H.; Nicolo, E. D.; Drioli, E.; Lee, Y. M. Understanding the Non-Solvent Induced Phase Separation (NIPS) Effect During the Fabrication of Microporous PVDF Membranes via Thermally Induced Phase Separation (TIPS). *J. Membr. Sci.* **2016**, *514*, 250−263.

(13) Fang, C.; Jeon, S.; Rajabzadeh, S.; Cheng, L.; Fang, L.; Matsuyama, H. Tailoring the Surface Pore Size of Hollow Fiber Membranes in the Tips Process. *J. Mater. Chem. A* **2018**, *6*, 535−547.

(14) Baker, R. W. Future Directions of Membrane Gas Separation Technology. *Ind. Eng. Chem. Res.* **2002**, *41*, 1393−1411.

(15) Wang, B.; Ji, J.; Li, K. Crystal Nuclei Templated Nano-structured Membranes Prepared by Solvent Crystallization and Polymer Migration. *Nat. Commun.* **2016**, *7*, No. 12804.

(16) Peinemann, K. V.; Abetz, V.; Simon, P. F. W. Asymmetric Superstructure Formed in a Block Copolymer via Phase Separation. *Nat. Mater.* **2007**, *6*, 992−996.

(17) Park, H. B.; Kamcev, J.; Robeson, L. M.; Elimelech, M.; Freeman, B. D. Maximizing the Right Stuff: The Trade-Off between Membrane Permeability and Selectivity. *Science* **2017**, *356*, 1138−1148.

(18) Jackson, E. A.; Hillmyer, M. A. Nanoporous Membranes Derived from Block Copolymers: From Drug Delivery to Water Filtration. *ACS Nano* **2010**, *4*, 3548−3553.

(19) Karunakaran, M.; Nunes, S. P.; Qiu, X.; Yu, H.; Peinemann, K. V. Isoporous PS-b-PEO Ultrafiltration Membranes via Self-Assembly and Water-Induced Phase Separation. *J. Membr. Sci.* **2014**, *453*, 471−477.

(20) Phillip, W. A.; O'Neill, B.; Rodwogin, M.; Hillmyer, M. A.; Cussler, E. L. Self-Assembled Block Copolymer Thin Films as Water Filtration Membranes. *ACS Appl. Mater. Interfaces* **2010**, *2*, 847−853.

(21) Nunes, S. P.; Behzad, A. R.; Hooghan, B.; Sougrat, R.; Karunakaran, M.; Pradeep, N.; Vainio, U.; Peinemann, K. V. Switchable pH-Responsive Polymeric Membranes Prepared via Block Copolymer Micelle Assembly. *ACS Nano* **2011**, *5*, 3516−3522.

DOI: 10.1021/acsami.8b16120
ACS Appl. Mater. Interfaces 2018, 10, 44041−44049

(22) Hahn, J.; Filiz, V.; Rangou, S.; Clodt, J.; Jung, A.; Buhr, K.; Abetz, C.; Abetz, V. Structure Formation of Integral-Asymmetric Membranes of Polystyrene-block-Poly(Ethylene Oxide). *J. Polym. Sci., Part B: Polym. Phys.* **2013**, *51*, 281−290.
(23) Rangou, S.; Buhr, K.; Filiz, V.; Clodt, J.; Lademann, B.; Hahn, J.; Jung, A.; Abetz, V. Self-Organized Isoporous Membranes with Tailored Pore Sizes. *J. Membr. Sci.* **2014**, *451*, 266−275.
(24) Nunes, S. P.; Sougrat, R.; Hooghan, B.; Anjum, D. H.; Behzad, A. R.; Zhao, L.; Pradeep, N.; Pinnau, I.; Vainio, U.; Peinemann, K. V. Ultraporous Films with Uniform Nanochannels by Block Copolymer Micelles Assembly. *Macromolecules* **2010**, *43*, 8079−8085.
(25) Qiu, X.; Yu, H.; Karunakaran, M.; Pradeep, N.; Nunes, S. P.; Peinemann, K. V. Selective Separation of Similarly Sized Proteins with Tunable Nanoporous Block Copolymer Membranes. *ACS Nano* **2013**, *7*, 768−776.
(26) Hahn, J.; Clodt, J.; Filiz, V.; Abetz, V. Protein Separation Performance of Self-Assembled Block Copolymer Membranes. *RSC Adv.* **2014**, *4*, 10252−10260.
(27) Matsuda, H.; Taniguchi, D.; Hashimoto, J.; Kurihara, K.; Ochi, K.; Kojima, K. Determination and Correlation of Liquid−Liquid Equilibria for Four Binary N,N-Dimethylformamide + Hydrocarbon Systems. *Fluid Phase Equilib.* **2007**, *260*, 81−86.
(28) Zhang, R.; Liu, Y.; He, M.; Su, Y.; Zhao, X.; Elimelech, M.; Jiang, Z. Antifouling Membranes for Sustainable Water Purification: Strategies and Mechanisms. *Chem. Soc. Rev.* **2016**, *45*, 5888−5924.
(29) Faraone, A.; Magazu, S.; Maisano, G.; Migliardo, P.; Tettamanti, E.; Villari, V. The Puzzle of Poly(Ethylene Oxide) Aggregation in Water: Experimental Findings. *J. Chem. Phys.* **1999**, *110*, 1801−1806.
(30) Li, Y. C.; Shi, R. P.; Wang, C. P.; Liu, X. J.; Wang, Y. Phase-Field Simulation of Thermally Induced Spinodal Decomposition in Polymer Blends. *Modell. Simul. Mater. Sci. Eng.* **2012**, *20*, No. 075002.
(31) Liu, J.; Lu, X. L.; Wu, C. R. Effect of Annealing Conditions on Crystallization Behavior and Mechanical Properties of NIPS Poly-(Vinylidene Fluoride) Hollow Fiber Membranes. *J. Appl. Polym. Sci.* **2013**, *129*, 1417−1425.
(32) Liu, J.; Lu, X. L.; Wu, C. R. Effect of Preparation Methods on Crystallization Behavior and Tensile Strength of Poly(Vinylidene Fluoride) Membranes. *Membranes* **2013**, *3*, 389−405.
(33) Liu, F.; Hashim, N. A.; Liu, Y.; Abed, M. M.; Li, K. Progress in the Production and Modification of PVDF Membranes. *J. Membr. Sci.* **2011**, *375*, 1−27.
(34) Ebert, K.; Fritsch, D.; Koll, J.; Tjahjawiguna, C. Influence of Inorganic Fillers on the Compaction Behaviour of Porous Polymer Based Membranes. *J. Membr. Sci.* **2004**, *233*, 71−78.
(35) Wang, P.; Ma, J.; Wang, Z.; Shi, F.; Liu, Q. Enhanced Separation Performance of PVDF/PVP-g-MMT Nanocomposite Ultrafiltration Membrane Based on the NVP-Grafted Polymerization Modification of Montmorillonite (MMT). *Langmuir* **2012**, *28*, 4776−4786.
(36) Razzaghi, M. H.; Safekordi, A.; Tavakolmoghadam, M.; Rekabdar, F.; Hemmati, M. Morphological and Separation Performance Study of PVDF/CA Blend Membranes. *J. Membr. Sci.* **2014**, *470*, 547−557.
(37) Rahimpour, A.; Madaeni, S. S. Polyethersulfone (PES)/Cellulose Acetate Phthalate (CAP) Blend Ultrafiltration Membranes: Preparation, Morphology, Performance and Antifouling Properties. *J. Membr. Sci.* **2007**, *305*, 299−312.
(38) Zhu, Y.; Xie, W.; Zhang, F.; Xing, T.; Jin, J. Superhydrophilic in-Situ-Cross-Linked Zwitterionic Polyelectrolyte/ PVDF-Blend Membrane for Highly Efficient Oil/Water Emulsion Separation. *ACS Appl. Mater. Interfaces* **2017**, *9*, 9603−9613.
(39) Arthanareeswaran, G.; Devi, T. K. S.; Raajenthiren, M. Effect of Silica Particles on Cellulose Acetate Blend Ultrafiltration Membranes: Part I. *Sep. Purif. Technol.* **2008**, *64*, 38−47.
(40) Aerts, P.; Greenberg, A. R.; Leysen, R.; Krantz, W. B.; Reinsch, V. E.; Jacobs, P. A. The Influence of Filler Concentration on the Compaction and Filtration Properties of Zirfon(R)-Composite Ultrafiltration Membranes. *Sep. Purif. Technol.* **2001**, *22-23*, 663−669.
(41) Bian, X.; Shi, L.; Yang, X.; Lu, X. Effect of Nano-TiO_2 Particles on the Performance of PVDF, PVDF-g-(Maleic Anhydride), and PVDF-g-Poly(Acryl Amide) Membranes. *Ind. Eng. Chem. Res.* **2011**, *50*, 12113−12123.
(42) Chen, W.; Su, Y.; Zhang, L.; Shi, Q.; Peng, J.; Jiang, Z. In Situ Generated Silica Nanoparticles as Pore-Forming Agent for Enhanced Permeability of Cellulose Acetate Membranes. *J. Membr. Sci.* **2010**, *348*, 75−83.
(43) Zhao, S.; Wang, Z.; Wei, X.; Zhao, B.; Wang, J.; Yang, S. Y.; Wang, S. Performance Improvement of Polysulfone Ultrafiltration Membrane Using Well-Dispersed Polyaniline−Poly-(Vinylpyrrolidone) Nanocomposite as the Additive. *Ind. Eng. Chem. Res.* **2012**, *51*, 4661−4672.
(44) Clodt, J.; Filiz, V.; Shishatskiy, S. Perfluorinated Compounds as Test Media for Porous Membranes. *Membranes* **2017**, *7*, 51.
(45) Kaner, P.; Rubakh, E.; et al. Zwitterion-Containing Polymer Additives for Fouling Resistant Ultrafiltration Membranes. *J. Membr. Sci.* **2017**, *533*, 141−159.

DOI: 10.1021/acsami.8b16120
ACS Appl. Mater. Interfaces 2018, 10, 44041−44049